Intermediate mass fragments emission in the reaction 47 MeV ^{7}Li + Mg

C. Bhattacharya, D. Bandyopadhyay, G.S.N. Murthy, Y.P. Viyogi, S.K. Basu, K. Krishan, and S. Bhattacharya
Variable Energy Cyclotron Centre, 1/AF Bidhan Nagar, Calcutta 700 064, India

S. Kailas, A. Chatterjee, and P. Singh
Nuclear Physics Division, Bhabha Atomic Research Centre, Bombay 400 085, India
(Received 21 March 1995)

The energy distributions of the intermediate mass fragments (IMF's, $4 \leq Z_{\mathrm{IMF}} \leq 9$) emitted in the reaction 47 MeV ^{7}Li + $^{\mathrm{nat}}$Mg have been measured in the angular range $15^{\circ} \leq \theta_{\mathrm{lab}} \leq 120^{\circ}$. Invariant cross sections plotted in the velocity plane have indicated the existence of a fusionlike source as well as some intermediate velocity source for lighter fragments. Source parameters for the fusionlike source and the intermediate velocity source have been extracted using the phenomenological moving source model. The results of the present measurement have been extensively compared with the predictions of the binary fragmentation model. The shapes of the fragment energy distribution have been reproduced fairly well by the binary fragmentation model except for the forward angle data for Be and B. The higher energy tails in the forward angle data for Be and B are indicative of the presence of other reaction processes. Average kinetic energies of the fragments and total elemental cross sections extracted from the data have been compared with those obtained from asymmetric binary fragmentation calculations. In both cases, it has been found that the theoretical predictions are in good agreement with the respective experimental estimates with the exception of Be and B, where the theory underpredicts the experimental results indicating additional contributions from other reaction mechanisms.

PACS number(s): 25.70.Jj, 25.70.Gh

I. INTRODUCTION

The study of reaction mechanisms for intermediate mass fragment (IMF) emission in low and intermediate energy nucleus-nucleus collisions is a subject of recent interest. A large number of inclusive as well as exclusive experiments have been done in recent years for different target-projectile combinations at various incident energies [1–30], to unfold the reaction mechanisms for IMF emission. From these efforts, the picture which emerges about the general features of IMF emission is as follows. (i) The IMF emission is a very general phenomenon and the mechanism of emission is different in different energy domains. (ii) At lower incident energies (i.e., typically below the Fermi energy domain), the nuclear mean field plays the most significant role in deciding the appropriate dynamics of IMF emission (binary decay [31–33]). (iii) At higher bombarding energies ($\gtrsim$ 50 MeV/nucleon), IMF's are emitted through multistep (sequential binary decay [34,35]) and/or single step (instantaneous multifragmentation [36]) processes and the main challenge, at present, is to resolve the ambiguities in the signatures of the two [23,24].

At lower bombarding energies, [$20 \lesssim E_{\mathrm{lab}}/A$ (MeV/nucleon)$\lesssim 50$], where incomplete fusion is dominant, the mass, charge, excitation energy, etc. of the fused composite, which undergoes binary fragmentation, are not uniquely determined. Rather, each of these variables has been found to have a fairly broad distribution [37], which complicates the analysis of the data. On the other hand, when the incident energy is $\lesssim$ 10 MeV/nucleon, incomplete fusion is negligible, and the fully equilibrated compound nucleus formed by complete fusion of projectile and target can be characterized by its mass and excitation energy. The IMF's emitted at these energies are expected to be predominantly of compound nuclear origin. However, there may be contributions from sources other than compound nuclear type, identification of which is essential for a better understanding of the mechanism of IMF emission in this energy domain.

Phenomenological analyses of the experimental heavy ion collision data indicate the presence of a number of sources contributing to IMF emission [38,39]. These sources can be broadly categorized as (i) fully equilibrated fusionlike sources moving with velocity close to compound nuclear velocity (v_{CN}), (ii) intermediate velocity sources (IVS's) having velocity lying between the projectile velocity v_p and v_{CN}, and (iii) projectilelike sources. It is, therefore, quite cumbersome to extract unambiguously the individual contributions for each of them. This information is, however, crucial to critically evaluate the roles played by various competing mechanisms proposed in the literature [40,41]. From this standpoint, lighter ion induced reactions have some advantages. IMF's emitted in lighter ion induced reactions are little contaminated by emission from projectilelike sources. Moreover, in this case, the products of deep inelastic scattering are easily distinguishable from those originating from fusion-fission reactions.

The aim of the present work is to study the mechanism of IMF emission from moderately "hot" nuclei where ambiguities due to competing reaction mechanisms

may be differentiated reasonably well. For this purpose, we have used 47 MeV ^{7}Li as projectile. At this energy, $E/A = 6.7$ MeV/nucleon, the incomplete fusion process is expected to be negligible [42]. Moreover, the IMF emission from projectilelike sources (quasielastic scattering, for example) is not significant except at forward angles ($\theta_{gr} \simeq 11°$) and massive transfer of nucleons from the target to the projectile (deep inelastic scattering) should not contribute significantly to IMF emission for $Z > 4$ [43]. In the present paper, we report the measurement of energy spectra and angular distributions for various IMF's ($4 \leq Z_{IMF} \leq 9$) emitted in the reaction ^{7}Li (47 MeV) + Mg.

The paper has been arranged as follows. In Sec. II, the experimental setup is described in brief. The experimental results are presented in Sec. III. In Sec. IV, the theoretical analysis of the data is discussed in detail. Finally, the summary and conclusion are given in Sec. V.

II. EXPERIMENTAL DETAILS

The experiment has been performed using a 47 MeV ^{7}Li beam from the Bhabha Atomic Research Centre—Tata Institute of Fundamental Research 14UD Pelletron accelerator laboratory, Bombay. The target was made of natural Mg having thickness 320 μg/cm^2. The beam size on the target was typically 1–1.5 mm wide and the beam current was 2–90 nA. The fragments were identified using a telescope consisting of a gas ΔE and a Si(Li) E (2 mm) detector. The gas ΔE detector was an ionization counter of axial configuration [44], and was filled with a continuous flow of $P10$ gas (90% Ar + 10% CH_4) at 90 Torr nominal pressure. Gas pressure was maintained constant to within ± 2 Torr. A thin polypropylene film of thickness 1.5 μm was used for the window of the gas detector. The gas telescope subtended a solid angle of 1.3 msr and had an angular opening of 1°. Analog signals from the detectors were processed using standard electronics before being fed to the computer for on-line data acquisition.

Carbon buildup on the target was monitored at regular intervals in the following manner. At forward angles (typically 40°), where Li elastic scattering from carbon and magnesium is kinematically well separated, the peak areas of the elastically scattered Li ions from the carbon deposited on Mg were extracted. These areas were then normalized with the same obtained from a pure carbon target of known thickness to estimate the thickness of carbon deposited on the Mg target. In addition, carbon buildup was also estimated from the elastic recoil peak of the carbon ejectile spectra. The two estimates were found to be in good agreement with one another. The thickness of the deposited carbon layer was estimated to be typically ~ 3.5 μg/cm^2, which increased to ~ 10 μg/cm^2 at the end of 96 h of the experimental run. The contamination of the continuum ejectile spectra due to this deposited carbon layer was also estimated and was found to be insignificant (for example, the carbon yield from a carbon target of thickness ~ 10 μg/cm^2 was measured to be $\lesssim 1\%$ of the same obtained from a Mg target).

The charge resolution obtained in this experiment is illustrated by the ΔE vs E plot displayed in Fig. 1. Well separated ridges are clearly seen corresponding to elements having atomic numbers up to Z =9. The telescope has been calibrated using elastically scatterd Li ion from C, Mg, and Au targets. Absolute energy calibrations of the E and ΔE detectors were done separately using standard kinematics and energy-loss calculations. Typical energy resolutions obtained in the calibration were 3.1% and 16% for E and ΔE, respectively. The measured energies have been corrected for the energy losses at the target and at the entrance window by incorporating a single average thickness correction for each fragment energy [17]. Experimental cutoffs thus obtained are typically 4 MeV for Be and 10 MeV for oxygen.

III. EXPERIMENTAL RESULTS

A. Inclusive energy distributions

Inclusive energy distribution for various fragments ($4 \leq Z \leq 9$) have been measured in the angular range of 15°–120° and are shown in Fig. 2. The error bars represent only statistical errors. The systematic errors in the data, arising out of the uncertainties in the measurements of solid angle, target thickness, and the calibration of the current digitizer have been estimated to be $\approx 10\%$. It is seen from Fig. 2 that, for all ejectiles except O and F, the slopes of the energy distributions change significantly as one goes from forward to backward angles. For these ejectiles, the energy spectra exhibit higher energy "tails," which are more pronounced at smaller angles. Furthermore, the contributions of the higher energy "tail" to the fragment energy distribution is most significant for the lightest fragments like Be and B, and it decreases for the heavier fragments. On the other hand, slopes of the energy distributions at backward angles are similar for all emitted fragments, consistent with the conjecture of emission from a fully equilibrated source.

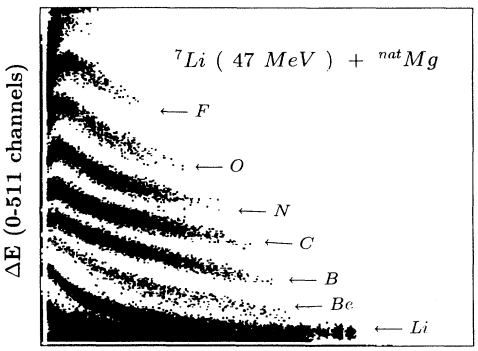

FIG. 1. E vs. ΔE plot for the reaction 47 MeV Li + Mg at the laboratory angle 40°.

B. Invariant cross sections

To have a better insight into the nature of emitting sources, the laboratory energy spectra have been transformed into invariant cross-section plots in velocity space. Figure 3 shows the plot of invariant cross-section contours as a function of velocities, parallel ($v_{\|}$) and perpendicular ($v_{\perp}$) to the beam direction for the fragments Be, B, C, N, O, and F, respectively. It is clear from this plot that the invariant cross sections (filled circles in Fig. 3, where larger sizes of circles correspond to higher cross-section bins) for heavier fragments (C, N, O, F) fall almost entirely on constant contour loci (semicircles) expected for isotropic emission from a source moving with an average velocity nearly equal to the compound nuclear velocity ($v_{CN} = 0.027c$, shown by the arrow in Fig. 3). In contrast, contours for the lighter fragments like Be and B are skewed to much larger velocities, indicating the presence of faster moving sources in addition to the compound nuclear source.

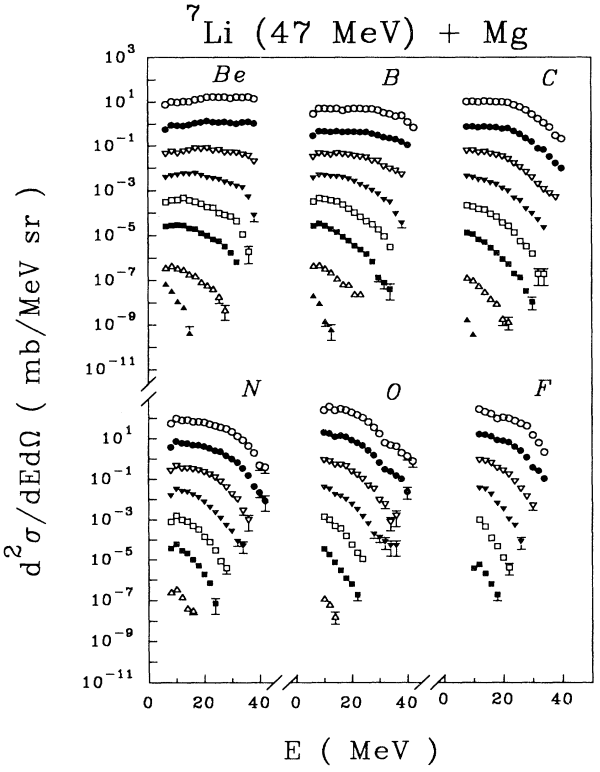

FIG. 2. $\frac{d^2\sigma}{dEd\Omega}$ for different fragments emitted in the reaction ^{7}Li (47 MeV) + Mg plotted as a function of the laboratory kinetic energy of the fragments. The open circle, filled circle, open inverted triangle, filled inverted triangle, open square, filled square, open triangle and filled triangle symbols correspond to the experimental data for the laboratory angles (multiplication factor) of 15°($\times 10^2$), 20°($\times 10^1$), 30°($\times 1$), 40°($\times 10^{-1}$), 50°($\times 10^{-2}$), 60°($\times 10^{-3}$), 70°($\times 10^{-4}$), and 120°($\times 10^{-5}$), respectively.

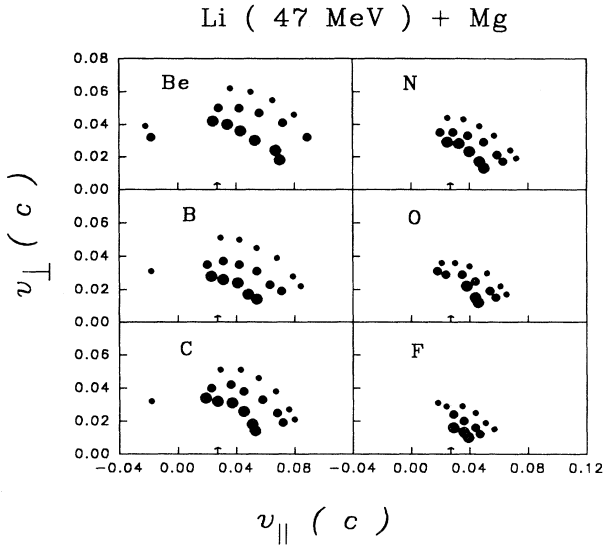

FIG. 3. Invariant cross sections for various fragments plotted as a function of velocities parallel ($v_{\|}$) and perpendicular ($v_{\perp}$) to the beam direction. Sizes of the filled circles are proportional to the cross sections. Arrow indicates the velocity of the compound nucleus.

C. Fragment average velocities

The average velocities of the fragments have been computed from the measured energies and from the Z values using the empirical mass formula proposed by Charity *et al.* [8]:

$$A = Z \times (2.08 + 0.0029 \times Z). \quad (1)$$

The average velocities have been plotted in the ($v_{\|}$) vs ($v_{\perp}$) plane in Fig. 4. It is seen that the average velocities

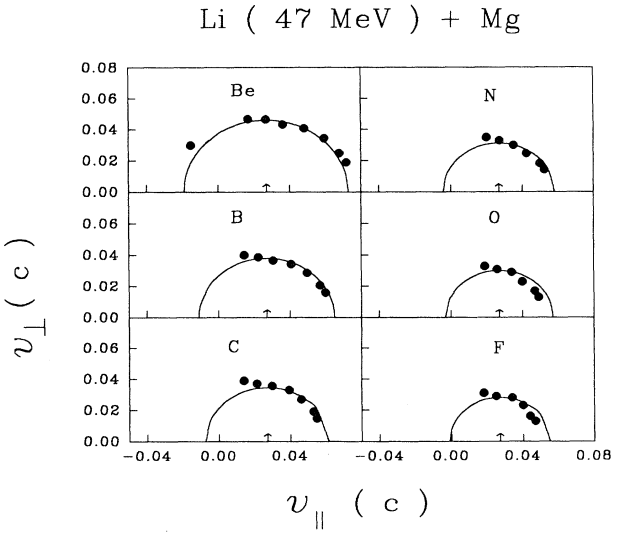

FIG. 4. Average velocities of various fragments plotted as a function of velocities parallel ($v_{\|}$) and perpendicular ($v_{\perp}$) to the beam direction. Arrow indicates the velocity of the compound nucleus.

fall on a circle centered around v_{CN}, which means that the average velocities (as well as kinetic energies) of the fragments are independent of the c.m. emission angles. It may be inferred from this analysis that for these reaction products energy relaxation is complete and the fragments are emitted from a fully equilibrated source moving with the CN velocity. The magnitude of the average fragment velocities (i.e., the radii of the circles in Fig. 4) increases with the decrease of fragment mass, which is indicative of the binary nature of the emission.

D. Total elemental cross sections

The total elemental cross sections $\sigma(Z)$, plotted as a function of atomic number Z of the detected fragments, has been displayed in Fig. 5. Filled circles represent the experimental estimates of $\sigma(Z)$, which have been obtained by integrating the energy spectra (Fig. 2) over the whole energy and angular range. The details of the integration procedure are given in Ref. [17]. The total uncertainties in the estimation of $\sigma(Z)$ due to experimental threshold and the limited angular range of the data have been estimated to be typically 14% for Be, 16% for B, 22% for C, 20% for N, 30% for O, and 27% for F. The cross section is found to vary between about 20 mb for Z =6 and about 5 mb for heavier (as well as lighter) fragments.

IV. ANALYSIS AND DISCUSSIONS

A. Phenomenological moving source model

To have a quantitative understanding of the nature of the sources, the present data have been fitted using a phenomenological moving source model where it is assumed that fragments are emitted isotropically in the rest frame of moving sources. In the laboratory frame, the double differential fragment emission cross sections can be written as

$$d^2\sigma/dEd\Omega = \sum_{i=1}^{N} C_i \Big[(E - E_B)E_i^s\Big]^{\frac{1}{2}} \exp(-E_i^s/T_i) \quad (2a)$$

with

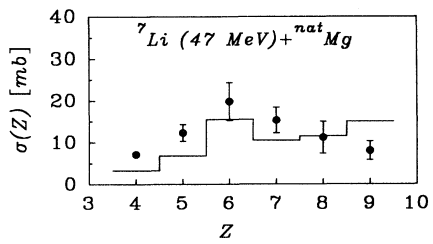

FIG. 5. Total elemental cross sections for different fragments plotted as a function of the fragment charge. Filled circles are the experimental data and the solid histogram is the theoretical calculation of the same (see text).

$$E_i^s = (E - E_B) + E_i - 2\Big[E_i(E - E_B)\Big]^{\frac{1}{2}} \cos\theta \quad (2b)$$

and

$$E_i = \frac{1}{2} m_f v_i^2, \quad (2c)$$

where E is the observed laboratory energy of the fragment of mass m_f at angle θ and E_B is the exit channel Coulomb barrier. The summation extends over the total number of sources N; C_i, v_i, and T_i correspond to the normalization constant, velocity, and temperature, respectively, for the ith source. In the present analysis, the number of sources has been restricted to only two; one intermediate velocity source (IVS) in addition to the equilibrated fusionlike source.

The source parameters for each fragment have been extracted in two steps in the following manner. In the first step, the energy spectra for each fragment at the backwardmost angles have been fitted using Eqs. (2) with a single equilibrated source with the assumption that at the backwardmost angles the emission is entirely from a fusionlike source. In the next step, the source parameters of the equilibrated, fusionlike source were kept fixed and the source parameters of the other faster moving source were extracted by two-source fitting of the forward angle ($\leq 60°$) data using Eqs. (2). The extracted source velocities and temperatures for different fragments are tabulated in Table I and the the fits thus obtained are shown in Fig. 6, where dashed and dotted curves correspond to the contributions of equilibrium (fusionlike) and intermediate velocity sources, respectively, and the solid curves are the sum total of the two. It is seen from Table I that the velocities of the fusionlike sources are slightly smaller and the velocities of the IVS's are considerably larger than the compound nuclear velocity (v_{CN} = 0.027c). The IVS source velocities for different fragments are nearly the same ($\sim$ 0.037c) with the exception of Be and B at 15°, where the source velocities are slightly larger. Since the present measurement is inclusive in nature, this may be due to some contributions from direct few-body transfer reactions, at forward angles. The temperature parameters corresponding to fusionlike as well as IV sources are found to vary with fragment mass. In both cases, the temperature is found to be minimum for the heaviest fragment and increases with decrease of the fragment mass. Similar variation of the temperature parameter has been reported earlier for the α + Al reaction [17,38]. For the fusionlike source, this may be intuitively understood as follows. Since the barrier height increases for the emission of heavier fragments, the corresponding available excitation energy in the exit channel (and *vis-à-vis* temperature) is smaller. The variation of the IVS temperature parameter with ejectile mass may be attributed to nonequilibrium reaction mechanisms [39]. The angle dependence of the IVS temperature parameter obtained in the present work is similar to the one obtained in the study of α particle induced reactions [38]. This may be due to the contributions to the fragment energy spectra from several

TABLE I. Source parameters for the fusionlike and intermediate velocity sources obtained from the phenomenological two-source analysis of the data.

Element	θ_{lab}	Fusionlike source		Intermediate velocity source	
	(deg)	v/c	T (MeV)	v/c	T (MeV)
Be	15	0.026 ± 0.003	2.4 ± 0.1	0.042 ± 0.004	7.9 ± 1.2
	30	0.026 ± 0.003	2.4 ± 0.1	0.038 ± 0.002	6.1 ± 0.2
	60	0.026 ± 0.003	2.4 ± 0.1	0.038 ± 0.003	3.3 ± 0.2
	120	0.026 ± 0.003	2.4 ± 0.1		
B	15	0.026 ± 0.002	2.3 ± 0.2	0.042 ± 0.003	3.8 ± 0.4
	30	0.026 ± 0.002	2.3 ± 0.2	0.038 ± 0.004	3.2 ± 0.3
	60,120	0.026 ± 0.002	2.3 ± 0.2		
C	15,30	0.026 ± 0.002	1.6 ± 0.1	0.037 ± 0.003	2.2 ± 0.3
	60	0.026 ± 0.002	1.6 ± 0.1		
N	15	0.026 ± 0.004	1.4 ± 0.2	0.037 ± 0.003	2.2 ± 0.3
	30,60	0.026 ± 0.004	1.4 ± 0.2		
O	All	0.026 ± 0.001	1.1 ± 0.1		
F	All	0.026 ± 0.001	0.9 ± 0.1		

nonequilibrium reaction mechanisms, as the data are inclusive in nature.

B. Binary fragmentation model

In recent years, asymmetric binary fragmentation of the compound nucleus [31,32] is considered as one of the dominant reaction mechanisms for the IMF emission in the low energy domain. According to this model, the emission of complex fragments may be thought of as a kind of fusion-fission process. In this scenario, the excited compound nucleus formed by the fusion of the two reactants undergoes dynamical deformation in the course of its time evolution. Subsequently it may enter into an exit channel configuration where the shape is deformed to look like a binary system connected by a small neck. With further deformation the neck ruptures, resulting in emission of two fragments. In this model there is no distinction between evaporation and fission. Therefore the formalism may be used for emission of all intermediate mass fragments from a compound nucleus.

1. Fragment energy spectra

The center of mass (c.m.) kinetic energy distribution of the binary fragments, according to a simplified version of Ref. [31], may be written as [7]

$$P(x)dx \sim \exp\left(-\frac{x}{T}\right), \tag{3}$$

where $x = E^{\rm kin}_{\rm c.m.} - E_B$, and E_B is the Coulomb barrier in the exit channel. Since there are several experimental indications that the exit channel is significantly deformed in the case of IMF emission (see Ref. [17] and references therein), exit channel deformation has to be properly incorporated in the calculation of E_B. The deformed barriers are calculated with the expression [17]

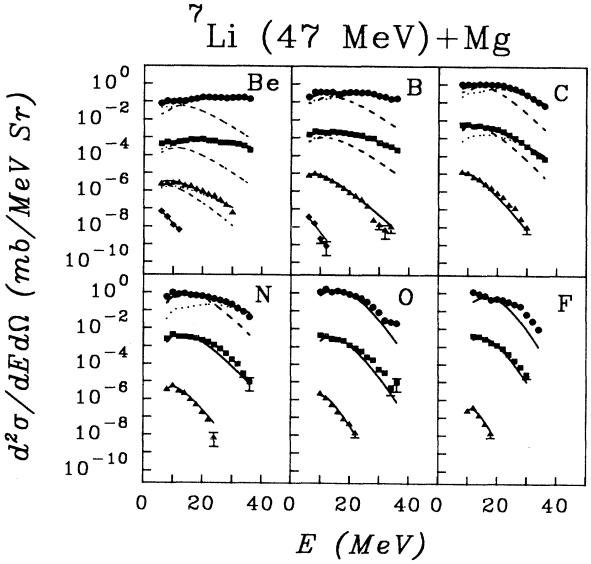

FIG. 6. $\frac{d^2\sigma}{dEd\Omega}$ for different fragments emitted in the reaction ^{7}Li (47 MeV) + Mg plotted as a function of the laboratory kinetic energy of the fragments. The filled circle, square, triangle, and diamond symbols correspond to the experimental data for the laboratory angles 15°, 30°, 60°, and 120° with multiplication factors of 1, 10^{-2}, 10^{-4}, and 10^{-6}, respectively. The dashed and dotted curves correspond to the contributions from fusionlike and intermediate velocity sources, respectively. The solid curve is the total contribution of the two sources.

$$E_B = \frac{Z_1 Z_2 e^2}{a_1 + a_2 + d} + \Delta W, \tag{4}$$

where Z_1,Z_2 and a_1,a_2 are the charges and semimajor axes of the two separating fragments where the fragments are taken to be prolate ellipsoids with their symmetry axes passing through the line joining the centers and d is the surface-to-surface separation distance at the conditional saddle point. The term ΔW is the higher order correction [17] to the barrier E_B.

Assuming an isotropic c.m. angular distribution, the c.m. energy spectrum [Eq. (3)] of the fragments can be transformed in the laboratory system using the following expressions [7]:

$$\frac{d^2P(E_L,\Omega_L)}{dE_L d\Omega_L} = \frac{k^2\sqrt{E_L}}{4\pi T^2}\left(\frac{A_{\rm CN}}{A_F E_{\rm CN}}\right)^{3/2} \times \frac{G(E_L,\theta_L)}{\left[G(E_L,\theta_L) + E_B/k\right]^{1/2}} \times \exp\left[-\frac{k}{T}G(E_L,\theta_L)\right] \tag{5a}$$

with

$$G(E_L,\theta_L) = \left(\sqrt{\frac{A_{\rm CN}E_L}{A_F E_{\rm CN}}} - \cos\theta_L\right)^2 + \sin^2\theta_L - \frac{E_B}{k} \tag{5b}$$

and

$$k = \frac{E_{\rm CN}A_F}{A_{\rm CN} - A_F}, \tag{5c}$$

where A_F, E_L, and θ_L are the mass number, energy, and emission angle of the detected fragment in the laboratory, and $E_{\rm CN}$ is the laboratory kinetic energy of the compound nucleus.

The predictions of the binary fragmentation model have been displayed in Fig. 7 along with respective experimental data for comparison. Assuming that the exit channel deformation is independent of the entrance channel so long as the mass and excitation energy of the compound nucleus are the same, the Coulomb barriers [Eq. (4)] have been calculated using the same deformation parameters as obtained earlier for (α+^{27}Al) [17]. It is clear from Fig. 7 that, except for the forward angle emission of lighter fragments like Be and B, the binary fragmentation model with the deformed barriers taken from [17] is found to reproduce the shape of the IMF energy distributions quite satisfactorily. This is indicative of the fact that the IMF emission is predominantly of compound nuclear origin and can be fairly well explained in terms of asymmetric binary splitting of a deformed compound system. However, the binary fragmentation picture alone cannot reproduce the shapes of the energy distribution for lighter fragments at forward angles. Therefore some other nonequilibrium reaction processes may also be contributing to the forward angle data. A similar observation has been made earlier in the analysis of IMF emission

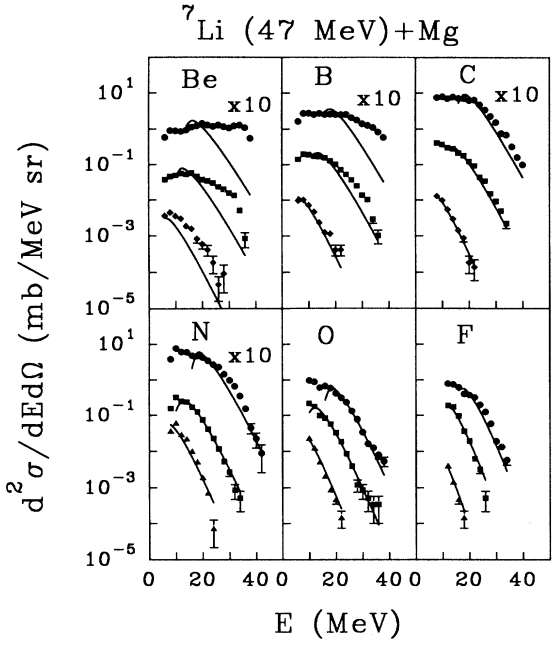

FIG. 7. $\frac{d^2\sigma}{dEd\Omega}$ for different fragments emitted in the reaction ^{7}Li (47 MeV) + Mg plotted as a function of the laboratory kinetic energy of the fragments. The filled circle, square, triangle, and diamond symbols correspond to the experimental data for the laboratory angles of 20°, 40°, 60°, and 70°, respectively. The solid curves are the results of the binary fragmentation model.

data from the α + Al reaction [17]. This is in agreement with the phenomenological moving source analysis (Sec. IV A) where it is shown that the shapes of the forward angle data for lighter fragments can only be reproduced with the incorporation of a second, faster moving source.

2. *Fragment average kinetic energy*

The process of fission may be thought of as a dynamical process consisting of a gradual change of shape, the formation of a neck, and finally separation into two fragments at the scission point. The IMF emission through binary fragmentation, which is essentially fission of nuclei below the Businaro-Gallone point [45], should therefore also have a similar evolution scenario. In the framework of a schematic dynamical model of IMF emission [46], we have calculated the mean kinetic energies of different fragments and compared them with the corresponding experimental estimates of the same.

Assuming that only a random fraction of the initial excitation energy of the compound nucleus goes to the collective degree of freedom to generate dynamics, the fission probability $P(f,\alpha|l)$ for any configuration α at angular momentum l is calculated from a Monte Carlo simulation of a large number of dynamical trajectories. Then the average kinetic energy $\langle E_k \rangle$ of the fragments

for the exit channel configuration α is calculated using the expression [46]

$$\langle E_k \rangle = \frac{\sum_{l=0}^{l_{cr}} (2l+1) E_k(\alpha) P(f,\alpha|l)}{\sum_{l=0}^{l_{cr}} (2l+1) P(f,\alpha|l)}, \quad (6)$$

where l_{cr} is the critical angular momentum for fusion [47]. The mean kinetic energies of the fragments calculated using Eq. (6) have been displayed in Fig. 8 along with the experimental estimates of the same for comparison. It is clearly evident from Fig. 8 that the theoretical predictions of $\langle E_k \rangle$ (solid curve) are in good agreement with the corresponding experimental results. For Be and B, the theoretical results slightly underpredict the experimental data. This further confirms the presence of some other mechanism in addition to fission in the case of Be and B, which has already been indicated in the analysis of Sec. IV A and Sec. IV B 1.

3. Total elemental cross section

In the framework of the binary fragmentation model, the total elemental IMF emission cross section can be calculated from simple phase-space considerations. Assuming that the reactants fuse completely to form an excited compound nucleus which subsequently decays statistically into various channels, the total emission cross section for a fragment of charge Z can be calculated using the expression [48]

$$\sigma(Z) = \pi \lambda^2 \sum_{l=0}^{l_{cr}} (2l+1) \frac{\Gamma_Z(l)}{\Gamma_{tot}}, \quad (7)$$

where λ is the de Broglie wavelength, $\Gamma_Z(l)$ is the decay width for the fragment of charge Z, and Γ_{tot} is the total decay width [48]. The ratio $\Gamma_Z(l)/\Gamma_{tot}$ represents the probability of decay of the compound nucleus of angular momentum l in a particular channel with charge Z.

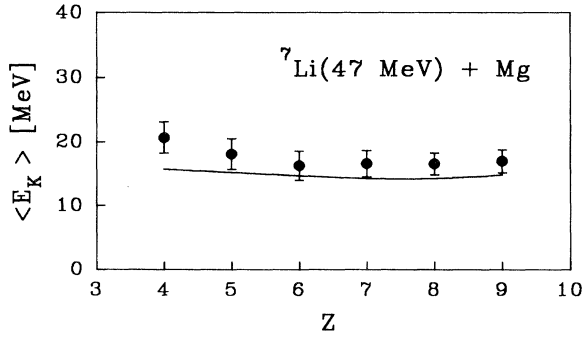

FIG. 8. Average kinetic energies for different fragments plotted as a function of the fragment charge. Filled circles are the experimental data and the solid curve is the theoretical calculation of the same (see text).

The decay width $\Gamma_Z(l)$, calculated in the transition state formalism [4], is given by

$$\Gamma_Z(l) \propto T_Z \left[\frac{E}{E - B_Z}\right]^2 \exp\left\{2[a(E-B_Z)]^{\frac{1}{2}} - 2(aE)^{\frac{1}{2}}\right\}, \quad (8)$$

where E is the compound nucleus excitation energy and B_Z is the barrier height at the conditional saddle point. The conditional saddle points have been derived by extremizing the potential energy of the deformed nuclear system [48]. The temperature T_Z is calculated from the relation $E - B_Z = aT_Z^2$, where a $(= A_{CN}/8)$ is the level density parameter. The prediction of the present calculations has been displayed in Fig. 5 by the solid histogram. It is seen that the total emission cross sections predicted by the present model are in good agreement with the corresponding experimental values except for lighter fragments where the theoretical predictions are seen to underestimate the experimental values. This may be indicative of the fact that heavier fragments are emitted from a nearly equilibrated compound nucleus, whereas processes other than purely statistical ones may play a signficant role in the emission of lighter fragments.

It may be noted here that, in the case of the α + Al reaction [17], the fragment yields have been satisfactorily explained within the framework of the binary fragmentation model. Recent studies by Anjos *et al.* [30] have shown that strongly energy damped fragment yields in the mass region $A_{CN} \sim 26$–29 may be satisfactorily explained in the framework of the fusion-fission model of Sanders [32], which is quite similar to the binary fragmentation model described in the present text; the two differ only in the parametrization of nuclear shapes and saddle point energies. It may, therefore, be inferred that the statistical fissionlike decay of the compound nucleus can consistently explain the observed yields of energy damped fragments in the low mass region around $A_{CN} \sim 26$–31.

V. SUMMARY AND CONCLUSION

The inclusive double differential cross sections for fragments ranging from Be to F emitted in the reaction ^{7}Li + Mg at 47 MeV have been measured. Total emission cross sections for various fragments emitted in the above reaction have been computed from the double differential cross-section data. From the rapidity analyses it has been found that the heavier fragments are emitted from a compound-nucleus-like source. On the other hand, the forward angle data for the lighter fragments are skewed to much larger velocities, indicating emission from faster moving sources. This is further supported by the phenomenological moving source analysis which indicates that different fragments are emitted from different sources. It has been found that the heavier fragments (C,N,O,F) as well as lighter fragments (Be,B) at backward angles are emitted from sources whose velocities are quite close to the compound nuclear velocity. The energy spectra for the lighter fragments, viz. Be

and B, at forward angles have been analyzed in terms of a two-source model which showed that in addition to a compound-nucleus-like source there are substantial contributions from an intermediate velocity source. The shapes of the energy distributions computed from the binary fragmentation model are also found to be in good agreement with the experimental data except for Be and B at forward angles. This is further indicative of the fact that forward angle data for lighter fragments have additional contributions from other reaction mechanisms. The average kinetic energies of the fragments calculated in the framework of the dynamical asymmetric fission model are also in good agreement with the respective experimental estimates of the same, again with the exception of Be and B, where the theory slightly underpredicts the experimental results. Total elemental cross sections for IMF emission also show a similar trend, where the data for the heavier fragments are fairly well explained, but the lighter fragment emission is underpredicted in the binary fragmentation model. It is clear from these observations that, though equilibrium processes dominate in this energy domain, the contributions of nonequilibrium processes are also quite significant.

To conclude, it is clear from the present study that the reaction process for IMF emission is predominantly binary in nature. Asymmetric binary splitting of the compound nucleus is able to explain satisfactorily most of the data. Energy distributions and mean kinetic energy of the fragments as well as total elemental cross sections can be fairly well explained with this model. For lighter fragments at forward angles, however, there may be some additional contributions from other sources, the origin of which may only be obtained from more exclusive experiments.

ACKNOWLEDGMENTS

The authors thank the Pelletron accelerator staff for the smooth running of the machine and D. C. Epraim for making the targets. One of the authors (K.K.) would like to thank Dr. J. P. Coffin of CNRS, Strasbourg for his interest in this work.

[1] C.B. Chitwood, D.J. Fields, C.K. Gelbke, W.G. Lynch, A.D. Panagiotou, M.B. Tasang, H. Utsunomiya, and W.A. Friedman, Phys. Lett. B **131**, 289 (1983).

[2] D.J. Fields, W.G. Lynch, C.B. Chitwood, C. K. Gelbke, M.B. Tasang, H. Utsunomiya, and J. Aichelin, Phys. Rev. C **30**, 1912 (1984).

[3] L.G. Sobotka, M.A. McMahan, R.J. McDonald, C. Signarbieux, G.J. Wozniak, M.L. Padgett, J.H. Gu, Z.H. Liu, Z.Q. Yao, and L.G. Moretto, Phys. Rev. Lett. **53**, 2004 (1984).

[4] M.A. McMahan, L.G. Moretto, M.L. Padgett, G.J. Wozniak, L.G. Sobotka, and M.G. Mustafa, Phys. Rev. Lett. **54**, 1995 (1985).

[5] K. Kwiatkowski, J. Bashkin, H. Karwowski, M. Fatyga, and V.E. Viola, Phys. Lett. B **171**, 41 (1986).

[6] D.J. Fields, W.G. Lynch, T.K. Nayak, M.B. Tsang, C.B. Chitwood, C.K. Gelbke, R. Morse, J. Wilczynki, T.C. Awes, R.L. Ferguson, F. Plasil, F.E. Obenshain, and G.R. Young, Phys. Rev. C **34**, 536 (1986).

[7] T. Kozik, J. Buschmann, K. Grotowski, H.J. Gils, N. Heide, J. Kiener, H. Klewe-Nebenius, H. Rebel, S. Zagromski, A.J. Cole, and S. Micek, Z. Phys. A **326**, 421 (1987).

[8] R.J. Charity, D.R. Bowman, Z.H. Liu, R.J. McDonald, M.A. McMahan, G.J. Wozniak, L.G. Moretto, S. Bradley, W.L. Kehoe, and A.C. Mignerey, Nucl. Phys. **A476**, 516 (1988).

[9] R.J. Charity, M.A. McMahan, G.J. Wozniak, R.J. McDonald, L.G. Moretto, D.G. Sarantites, L.G. Sobotka, G. Guarino, A. Pantaleo, L. Fiore, A. Gobbi, and D. Hildenbrand, Nucl. Phys. **A483**, 371 (1988).

[10] D.E. Fields, K. Kwiatokowski, D. Bonser, R.W. Viola, V.E. Viola, W.G. Lynch, J. Pochodzalla, M.B. Tsang, C.K. Gelbke, D.J. Fields, and S.M. Austin, Phys. Lett. B **220**, 356 (1989).

[11] K. Grotowski, J. Ilnicki, T. Kozik, J. Lukasik, S. Micek, Z. Sosin, A. Wieloch, N. Heide, H. Jelitto, J. Kiener, H. Rebel, S. Zagromski, and A.J. Cole, Phys. Lett. B **223**, 287 (1989).

[12] H.Y. Han, K.X. Jing, E. Plagnol, D.R. Bowman, R.J. Charity, L. Vinet, G.J. Wozniak, and L.G. Moretto, Nucl. Phys. **A492**, 138 (1989).

[13] H.M. Xu, W.G. Lynch, C.K. Gelbke, M.B. Tsang, D.J. Fields, M.R. Maier, D.J. Monissey, T.K. Nayak, J. Pochodzalla, D.G. Sarantites, L.G. Sobotka, M.L. Halbert, and D.C. Hensley, Phys. Rev. C **40**, 186 (1989).

[14] Y.D. Kim, M.B. Tsang, C.K. Gelbke, W.G. Lynch, N. Carlin, Z. Chen, R. Fox, W.G. Gong, T. Murakami, T.K. Nayak, R.M. Ronningen, H.M. Xu, F. Zhu, W. Bauer, L.G. Sobotka, D. Stracener, D.G. Sarantites, Z. Majka, V. Abenanta, and H. Griffin, Phys. Rev. Lett. **63**, 494 (1989).

[15] N.H. Papadakis, N.P. Vodinas, Y. Cassagnou, R. Dayras, R. Fonte, G. Imme, R. Legrain, A.D. Panagiotou, E.G. Pollacco, G. Reciti, G. Rodriguez, F. Saint-Laurent, M.G. Saint-Laurent, and N. Saunier, Phys. Lett. B **240**, 317 (1990).

[16] R.J. Charity, K.X. Jing, D.R. Bowman, M.A. McMahan, G.J. Wozniak, L.G. Moretto, N. Colonna, G. Guarino, A. Pantaleo, L. Fiore, A. Gobbi, and D. Hildenbrand, Nucl. Phys. **A511**, 59 (1990).

[17] C. Bhattacharya, S.K. Basu, S. Bhattacharya, A. Chakraborty, S. Chattopadhyay, M.R. Dutta Majumdar, K. Krishan, G.S.N Murthy, B. Sinha, M.D. Trivedi, Y.P. Viyogi, S.K. Dutta, and R.K. Bhowmik, Phys. Rev. C **44**, 1049 (1991).

[18] D.R. Bowman, G.F. Peaslee, R.T. de Souza, N. Carlin, C.K. Gelbke, W.G. Gong, Y.D. Kim, M. Lisa, W.G. Lynch, L. Phair, M.B. Tsang, C. Williams, N. Colona, K. Hanold, M.A. McMahan, G.J. Wozniak, L.G. Moretto,

and W.A. Friedman, Phys. Rev. Lett. **67**, 1527 (1991).
[19] D.N. Delis, Y. Blumenfeld, D.R. Bowman, N. Colonna, K. Hanold, K. Jing, M. Justice, J.C. Meng, G.F Peaslee, G.J. Wozniak, and L.G. Moretto, Nucl. Phys. **A534**, 403 (1991).
[20] R.T. de Souza, L. Phair, D.R. Bowman, N. Carlin, C.K. Gelbke, W.G. Gong, Y.D. Kim, M. Lisa, W.G. Lynch, G.F. Peaslee, M.B. Tsang, H.M. Xu, F. Zhu, and W.A. Friedman, Phys. Lett. B **268**, 6 (1991).
[21] J. Hubele, P. Kreutz, J.C. Adloff, M. Begemann-Blaich, P. Bouissou, G. Imme, I. Iori, G.J. Kunde, S. Leray, V. Lindenstruth, Z. Liu, U. Lynen, R. Meijer, U. Milkau, A. Moroni, W.F.J Muller, C. Ngo, C.A. Ogilvie, J. Pochodzalla, G. Reciti, G. Rudolf, H. Sann, A. Schuttauf, W. Seidel, L. Stuttge, W. Trautmann, and A. Tucholski, Z. Phys. A **340**, 263 (1991).
[22] S.J. Yennello, E.C. Pollacco, K. Kwiatkowski, C. Volant, R. Dayras, Y. Cassagnou, R. Legrain, E. Norbeck, V.E. Viola, J.L. Wile, and N.R. Yoder, Phys. Rev. Lett. **67**, 671 (1991).
[23] K. Hagel, M. Gonin, R. Wada, J.B. Natowitz, B.H. Sa, Y. Lou, M. Gui, D. Utley, G. Nebia, D. Fabris, G. Prete, J. Ruiz, D. Drain, B. Chambon, B. Cheynis, D. Guinet, X.C. Hu, A. Demeyer, C. Pastor, A. Giorni, A. Lleres, P. Stassi, J.B. Viano, and P. Gonthier, Phys. Rev. Lett. **68**, 2141 (1992).
[24] G. Bizard, D. Durand, A. Genoux-Lubain, M. Louvel, R. Bougalt, R. Brou, H. Doubre, Y. El-Masri, H. Fugiwara, K. Hagel, A. Hajfani, F. Hanappe, S. Jeong, G.M. Jin, S. Kato, J.L. Laville, C. Le Brun, J.F. Lecolley, S. Lee, T. Matsuse, T. Motobayashi, J.P. Party, A. Peghaire, J. Peter, N. Prot, R. Regimbart, F. Saint-Laurent, J.C. Stockmeyer, and B. Tamain, Phys. Lett. B **276**, 413 (1992).
[25] C. Beck, B. Djerroud, F. Haas, R.M. Freeman, A. Hachem, B. Heusch, A. Morsad, M. Youlal, Y. Abe, A. Dayras, J.P. Wieleczko, B.T. Matsuse, and S.M. Lee, Z. Phys. A **343**, 309 (1992).
[26] K. Yuasa-Nakagawa, Y.H. Pu, S.C. Jeong, T. Mizota, Y. Futami, S.M. Lee, T. Nakagawa, B. Heusch, K. Ieki, and T. Matsuse, Phys. Lett. B **283**, 185 (1992).
[27] L.W. Woo, K. Kwiatkowski, W.G. Wilson, V.E. Viola, H. Breuer, and G.J. Mathews, Phys. Rev. C **47**, 267 (1993).
[28] D. Prindle, R. Vandenbosch, S. Kailas, A. Charlop, and C. Hyde-Wright, Phys. Rev. C **48**, 291 (1993).
[29] J. Boger, J.M. Alexander, A. Elmaani, S. Kox, R.A. Lacey, A. Narayanan, D.J. Moses, M.A. Mcmahan, P.A. DeYoung, and C.J. Gelderloos, Phys. Rev. C **49**, 1576 (1994).
[30] R.M. Anjos, N. Added, N. Carlin, L. Fante, Jr., M.C.S. Figueira, R. Matheus, E.M. Szanto, C. Tenrein, A. Szanto de Toledo, and S.J. Sanders, Phys. Rev. C **49**, 2018 (1994).
[31] L.G. Moretto, Nucl. Phys. **A247**, 211 (1975).
[32] S.J. Sanders, Phys. Rev. C **44**, 2676 (1991).
[33] S.M. Lee, W. Yokota, and T. Matsuse, in Proceedings of the Symposium on the Many Facets of Heavy-Ion Fusion Reactions, Argonne, 1986, edited by D.G. Kovar, Argonne National Laboratory Report No. ANL-PhY-86-1, 1986, p. 63.
[34] W.A. Friedman and W.G. Lynch, Phys. Rev. C **28**, 16 (1983).
[35] J. Richert and P. Wagner, Nucl. Phys. **A517**, 399 (1990).
[36] D.H.E. Gross, Rep. Prog. Phys. **53**, 605 (1990), and references therein.
[37] C. Bhattacharya, S. Bhattacharya, and K. Krishan, Phys. Rev. C **49**, 3147 (1994).
[38] C. Bhattacharya, S. Bhattacharya, and K. Krishan, Z. Phys. A **346**, 281 (1993).
[39] B. Borderie, J. Phys. (Paris) Colloq. **47**, C4-251 (1986), and references therein.
[40] L.G. Moretto and G.J. Wozniak, Annu. Rev. Nucl. Part. Sci. **43**, 379 (1993), and references therein.
[41] B. Shivakumar, S. Ayik, B.A. Harmon, and D. Shapira, Phys. Rev. C **35**, 1730 (1987).
[42] H. Morgenstern, W. Bohne, W. Galster, K. Grabisch, and A. Kyanowski, Phys. Rev. Lett. **52**, 1104 (1984).
[43] R. Bass, *Nuclear Reactions with Heavy Ions* (Springer-Verlag, Berlin, 1980), p. 213.
[44] S.K. Bandyopadyay, S.K. Basu, S. Bhattacharya, R.K. Bhowmik, A. Chakrabarty, S.K. Datta, G.S.N. Murthy, and Y.P. Viyogi, Nucl. Instrum. Methods Phys. Res. Sect. A **278**, 467 (1989).
[45] U.L. Businaro and S. Gallone, Nuovo Cimento **1**, 629 (1955); **1**, 1277 (1955).
[46] A. Dhara, C. Bhattacharya, S. Bhattacharya, and K. Krishan, Phys. Rev. C **48**, 1910 (1993).
[47] R. Bass, *Nuclear Reactions with Heavy Ions* [43], p. 256.
[48] C. Bhattacharya and S. Bhattacharya, Phys. Rev. C **43**, 1491 (1991).